

# Medical Image Fusion in Oversampled Graph Filter Banks

Min-Sung Koh

Department of Engineering and Design, School of Computing and Engineering Sciences, Eastern Washington University Cheney, WA 99004, USA  
Email: mkoh@ewu.edu

**Abstract**—Recently, oversampled graph filter banks (OSGFBs) have been constructed on graph theory for signal processing in [1]-[7]. This paper introduces a new image fusion for medical images in OSGFBs. Images are decomposed to subband images by spectral graph wavelet transform in OSGFBs, revised by a simple fusion rule, and synthesized back to make a fused image. Since the OSGFBs have good capability to decompose regular/irregular signals, the proposed algorithm shows better performance than traditional fusion algorithms even with a simple fusion rule. The proposed algorithm is effective particularly for medical images. Visual and numerical performance comparisons of the proposed algorithm with traditional image fusion algorithms are included for medical, multifocus, and infrared images.

**Index Terms**—image fusion, graph filter banks, medical images, oversampled, graph signal processing

## I. INTRODUCTION

Traditional signal analysis and processing techniques such as wavelets, Fourier analysis, etc., are well designed to handle regular signals (e.g., images and videos etc.). However, it is a challenging task to apply the traditional signal processing techniques to irregular signals obtained through world-wide web, social network, traffic network, power grid, biological systems etc. In order to deal with those irregular signals, graph theories have recently been merged to signal processing in [1]-[7]. Good tutorials for graph signal processing are in [2], [3]. Particularly, traditional filter bank theory in wavelets has been evolved for graphs as well in [1], [4] and extended to oversampled cases in [6], [7]. The Graph Filter Banks (GFBs) introduced in [1], [4], [6], [7] are based on a Laplacian matrix, which is attained through an adjacent matrix representing connectivity of each node in a graph. The (OS) GFBs are applicable to regular/irregular signals and show outperforming results to wavelet filter banks [4], [6], [7] even for regular signals. Traditional signal analysis techniques such as discrete Fourier transform, Discrete Wavelet Transform (DWT), Curvelet Transform (CVT), Nonsubsampled Contourlet Transform (NSCT) etc., have been essential for many applications such as image fusion, image denoising/enhancement etc. Image fusion is to integrate many images taken from multiple image sensors,

temporal views, and/or limited optical lenses etc., in order to get a single image, which can be better recognized by human beings and/or machines [8]. Image fusion has been studied for medical applications, security surveillance, computer visions, astronomy, and remote sensing etc. Many image fusion algorithms in frequency domain have a mainstream concept: transforming images to frequency domain, modifying coefficients in frequency domain based on fusion rules, and transforming it back to temporal domain. The common concept was implemented with various different transforms such as DWT [9], NSCT [10], [11], CVT [12]-[14] etc. This paper applies Spectral Graph Wavelet Transform (SGWT) [15] in OSGFBs with a simple fusion rule choosing maximum transform coefficients. Even with the simple fusion rule, the proposed fusion algorithm in OSGFBs shows outperforming results to other image fusion algorithms based on DWT and CVT. This paper will introduce a new image fusion algorithm as follows: Section II introduces OSGFBs, and Section III explains a simple fusion rule applied in OSGFBs. Experimental results for medical, multifocus, and infrared images are shown in Section IV. Conclusions are followed in Section V.

## II. OVERSAMPLED GRAPH FILTER BANKS

Graph signal processing is formulated on a matrix called adjacency matrix expressing connectivity of each node in regular/irregular signals [1]-[7]. Let's consider a graph denoted by  $\mathcal{G} = \{\mathcal{V}, \mathcal{E}\}$ , where  $\mathcal{V}$  and  $\mathcal{E}$  respectively denote sets of nodes and edges in a graph. To make the adjacency matrix,  $A_0$ , from an undirected graph having the same weight of 1, equation (1) is defined [1], [4], [6], [7], [15]:

$$A_0(m, n) = \begin{cases} 1 & \text{if nodes } m \text{ and } n \text{ are connected,} \\ 0 & \text{otherwise} \end{cases} \quad (1)$$

In (1),  $A_0(m, n) \in \mathfrak{R}^{N_0 \times N_0}$  implies a (m, n) element in the adjacency matrix,  $A_0$ , where  $N_0$  is a number of nodes in a given graph. For instance,  $N_0 = MN$  for a ( $M \times N$ ) image. Using the adjacency matrix, the normalized Laplacian matrix denoted by  $L$  is calculated as (2) [15]:

$$L = D^{-\frac{1}{2}}(D - A_0)D^{-\frac{1}{2}} \quad (2) \\ = I - D^{-\frac{1}{2}}A_0D^{-\frac{1}{2}}$$

where  $D$  is a diagonal matrix obtained by  $D(m, m) = \sum_n A_0(m, n)$ . Many topics of graph signal processing

such as graph frequencies, graph Fourier transform etc., are related to the eigenvalue problems of the Laplacian matrix [1]-[7], [15]. Like traditional wavelet filter banks, perfectly reconstructable GFBs were developed in [1] for orthogonal cases and in [4] for biorthogonal cases with down/up sampling concepts utilizing node colors. The GFBs developed in [1], [4] are all critically sampled GFBs. Those critically sampled GFBs, which are designed with bipartite subgraphs, show similar filter bank structures to wavelet filter banks [1], [4]. Any image can be modeled as a 4 colorable graph [1], [4], [6], [7], and critically sampled GFBs can handle 4 colorable graphs (i.e., images) with rectangular and diagonal subgraphs within a similar structure to wavelet filter banks. Although GFBs have a similar structure to wavelet filter banks, GFBs are different in designed analysis/synthesis filters for graph signals and in down/up sampling for colors [1]-[7]. Analysis / synthesis filters in GFBs are newly designed for graph signals by considering the various constraints such as perfect reconstruction, zero DC responses etc., [1], [4]. Since oversampled filter banks are effective in some applications such as signal analysis, denoising etc., those critically sampled GFBs were extended to OSGFBs in [6], [7] with an idea to append additional nodes while keeping bipartite subgraphs. Since a rectangular subgraph can be oversampled by appending same nodes with a diagonal subgraph in images (or vice versa), an efficient oversampling was achieved in [6], [7]. With the simple efficient oversampling in [6], [7], all nodes in bipartite subgraphs (i.e., rectangular and diagonal subgraphs) are processed at the same time in OSGFBs, and it leads to an effective finer signal decomposition as shown in [6], [7]. To decompose images in OSGFBs, a revised adjacency matrix must be provided because appended nodes for oversampling are considered as well. It can be obtained through (3) [6], [7]:

$$\tilde{A} = \begin{bmatrix} A_0 & A_{01} \\ A_{01}^T & 0_{N-N_0} \end{bmatrix} \in \mathfrak{R}^{N \times N} \quad (3)$$

where  $A_0$  is the original adjacency matrix in (1), which is obtained from a given graph, and  $A_{01}$  is an adjacency matrix of appended nodes for oversampling. Notice  $0_{N-N_0}$  is a zero matrix of  $(N - N_0) \times (N - N_0)$ . Using the revised adjacency matrix  $\tilde{A}$  in (3), the revised Laplacian matrix for OSGFBs is calculated by (4), which is similar to (2) [6], [7]:

$$\begin{aligned} \tilde{L} &= \tilde{D}^{-\frac{1}{2}}(\tilde{D} - \tilde{A})\tilde{D}^{-\frac{1}{2}} \\ &= I - \tilde{D}^{-\frac{1}{2}}\tilde{A}\tilde{D}^{-\frac{1}{2}} \end{aligned} \quad (4)$$

where  $\tilde{D}$  is a diagonal matrix calculated by  $\tilde{D}(m, m) = \sum_n \tilde{A}(m, n)$ . The revised Laplacian matrix,  $\tilde{L}$ , is then applied to the SGWT as given in (5) [1], [15]:

$$T_g \mathbf{f} = \sum_{k=1}^N g(\lambda_k) \tilde{f}(k) \mathbf{u}_k \quad (5)$$

where  $\mathbf{f} = [\mathbf{f}_0; \mathbf{f}_1] \in \mathfrak{R}^{N \times 1}$  is an oversampled graph signal vector in this paper and  $T_g = g(\tilde{L})$  is a graph wavelet operator with a spectral graph kernel function,  $g$ , behaving a bandpass filter [15]. In making the

oversampling graph signal,  $\mathbf{f}$ , a given image is changed to a vector,  $\mathbf{f}_0 \in \mathfrak{R}^{N_0 \times 1}$ , and a clever way in [7] to choose appended graph signal,  $\mathbf{f}_1 \in \mathfrak{R}^{N_1 \times 1}$ , is used in this paper. In equation (5),  $\tilde{f}$  is a graph Fourier transform defined in [1], [6], [15], and  $\mathbf{u}_k$  is the  $k$ th eigenvector of  $\tilde{L}$  in (4). The graph wavelet operator can be approximated by  $k$  degree polynomials such as  $T_{\tilde{g}} = \hat{g}(\tilde{L}) = \sum_{l=0}^k a_l \tilde{L}^l$  (e.g., Chebyshev polynomials) [1], [15]. A computationally efficient calculation of (5) utilizing approximate  $T_{\tilde{g}}$  in a Chebyshev recurrence form is shown in [15]. With scaled bandpass kernels,  $g(t\lambda)$ , other low pass kernels denoted by  $h(\lambda)$  were originally designed to satisfy perfect reconstruction and zero DC responses for critically sampled GFBs [1], [4]. The same concept is extended to design M-channel GFBs in [6] and leads to OSGFBs in [7], which is implemented in this paper for an image fusion application. The OSGFBs applied to image fusion in this paper is shown in Fig. 1, where  $H_i$  for  $i=0, 1, 2, 3$  and  $G_i$  – which are filters in corresponding synthesis OSGFBs – are perfectly reconstructable graph filters designed in [6], [7] for oversampled graph signals.

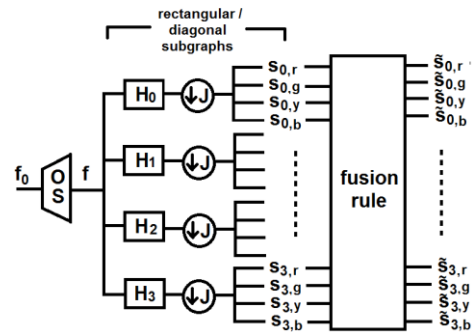


Figure 1. One decomposition level of analysis OSGFBs for image fusion.

In Fig. 1,  $J$  implies down sampling for each color and  $OS$  implies oversampling. Notice OSGFBs can process an image in rectangular and diagonal direction at the same time using the appended graph signal. In Fig. 1,  $\mathbf{f}$  is simply made by  $\mathbf{f} = [\mathbf{f}_0; \mathbf{f}_1]$ , where  $\mathbf{f}_1 = \mathbf{f}_0$ , for oversampling. However, notice that  $A_0$  for  $\mathbf{f}_0$  and  $A_{01}$  for  $\mathbf{f}_1$  are obtained from a rectangular subgraph and a diagonal subgraph respectively. Those oversampled settings provide finer eigenvalues of Laplacian matrix as well as simultaneous processing of each node in rectangular and diagonal connections [6], [7]. Notice that the finer eigenvalues of Laplacian matrix affect the SGWT in (5). Since any image can be expressed by bipartite subgraphs having 4 different color nodes, the  $i$ th subband graph signal (i.e.,  $i$ th subband image) is denoted by  $s_{i,c}$ , where  $c \in \{r, g, y, b\}$  for red, green, yellow, and blue color nodes respectively in an image. In Fig. 1,  $s_{i,c}$  stands for color nodes,  $c$ , in the  $i$ th subband signal. In this paper, notices that total 16 subband graph signals of  $s_{i,c}$  are available even at the decomposition level of 1 because 4-channel OSGFBs are used. For an image fusion application, the final edge is obtained through AND operation of edges in two input images. Notice in Fig. 1 that  $A_0$  matrix is constructed by applying edge-aware

image graph in [16] to an averaged image of two input images. Each subband graph signal obtained through Fig. 1 is shown in Fig. 2. In Fig. 2, all subband graph signals are obtained for a medical image given in Fig. 3 through 64 x 64 block processing to avoid too big matrix size of  $\tilde{L}$  in (4).

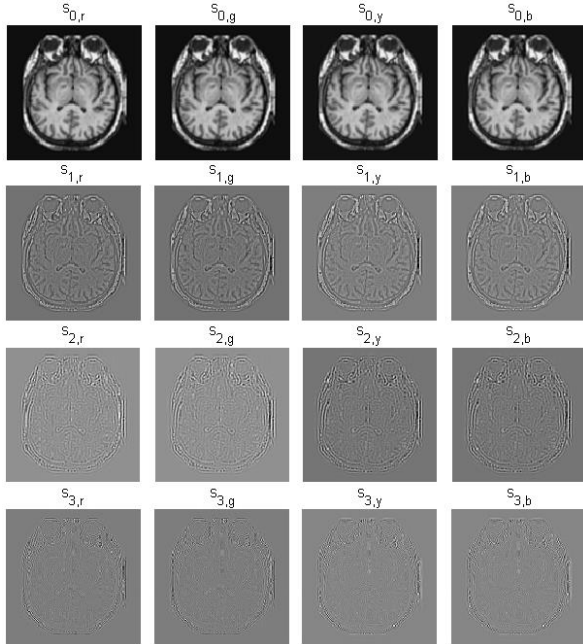


Figure 2. All subband graph signals,  $s_{i,c}$ , obtained through Fig. 1.

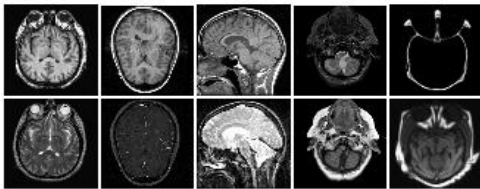


Figure 3. Medical images tested for image fusion in OSGFBs of Fig. 1.

### III. A FUSION RULE IN OSGFBs

In this paper, all subband signals in Fig. 2 are modified through a simple fusion rule. Many different fusion rules have been proposed as given in [8]-[14] in order to modify transform coefficients using pixel by pixel processing and/or using the information (e.g., activities) of neighboring pixels. Most fusion algorithms use two different ways: one for the lowest frequency subband and the other for high frequency subbands. For instance, averaging without a threshold [10] or with a threshold [11], inter-subband consistency [14], and sparse representation [8] were used for the lowest frequency subband, to name a few. Choosing maximum magnitude of transform coefficients was widely employed for high frequency subbands utilizing region energy of neighboring pixels [10], directional contrasts [11], transform coefficients of each pixel [8], [14]. In this paper, a simple rule choosing maximum magnitude of graph wavelet coefficients in OSGFBs is adopted for high frequency subbands, and averaging of two graph wavelet coefficients is used for the lowest frequency subband as given in (6) and (7):

$$\tilde{s}_{0,r} = (s_{0,r}^A + s_{0,r}^B)/2 \quad (6)$$

$$\tilde{s}_{i,c} = \begin{cases} s_{i,c}^B & \text{if } |s_{i,c}^B| \geq |s_{i,c}^A| \\ s_{i,c}^A & \text{otherwise} \end{cases} \quad (7)$$

where  $i = 0,1,2,3$ ,  $c \in \{r, g, y, b\}$ , except for  $\tilde{s}_{0,r}$ .

In (6) and (7), notice that two equations are applied to every node in each color, where superscript A and B imply two given input images for fusion processing. Equation (6) is for the lowest frequency subband,  $\tilde{s}_{0,r}$ , and equation (7) is for other high frequency subbands in OSGFBs. The modified graph wavelet coefficients through (6) and (7) are denoted by  $\tilde{s}_{i,c}$  in Fig. 1. After applying the fusion rule, those  $\tilde{s}_{i,c}$  subband signals pass through synthesis OSGFBs to obtain a fused image. Synthesis OSGFBs have the exact same structure with Fig. 1 except for  $G_i$ , up-samplers, and under-sampling parts which are counterparts corresponding to  $H_i$ , downsamplers, and oversampling respectively. In other words, under-sampling in synthesis OSGFBs is the counterpart of OS in Fig. 1 to make the same length of signal with that of the original signal,  $f_0$ . In this paper, under-sampling is achieved by equation (8), which is an average of two fused signals:

$$\hat{f}^{fused} = (\hat{f}_0^{fused} + \hat{f}_1^{fused})/2 \quad (8)$$

In (8), notice  $\hat{f}_0^{fused}$  and  $\hat{f}_1^{fused}$  respectively denote a fused graph signal for original and appended images in OSGFBs.

### IV. EXPERIMENTAL RESULTS

The proposed fusion algorithm is tested for 10 medical images (i.e., 5 pairs for the image fusion) as given in Fig. 3.

Images in the first and second row of Fig. 3 respectively imply the subscript "A" and "B" in (6) and (7). To begin with, two pair images denoted by "A" and "B" are respectively decomposed through OSGFBs in Fig. 1. Then, the SGWT coefficients in the same subbands of "A" and "B" are fused by (6) and (7) in this paper. As the last step, the final fused image is obtained by (8) after passing through synthesis OSGFBs. The results in this paper are compared with other traditional image fusion algorithms utilizing DWT [9] and CVT [13]. The results of fused images are given in Fig. 4. As shown in Fig. 4, the proposed algorithm outperforms two other fusion algorithms even with the simple fusion rule in (6) and (7). For fair comparison, decomposition level for DWT is set as 4, and the number of scales for CVT is also set as 4 (i.e., it means 5 including the coarsest scale) to obtain Fig. 4. Whereas, notice that the proposed algorithm is kept with decomposition level of 1 to obtain Fig. 4, because OSGFBs in Fig. 1 have total 16 subbands even at decomposition level of 1. Since OSGFBs are providing finer spectral wavelet coefficients with simultaneous process of rectangular and diagonal subgraphs [6], [7], the results of the proposed fusion algorithm in Fig. 4 show clearer images than DWT and CVT fusion algorithms. Visually, the proposed algorithm brings to better perception in Fig. 4.

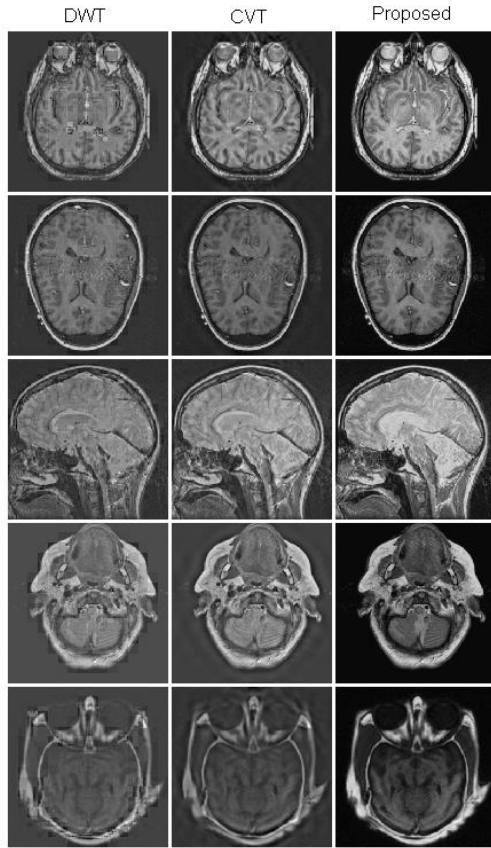


Figure 4. Fusion results for the test images in Fig. 3.

TABLE I. PERFORMANCE COMPARISON FOR MEDICAL IMAGES DECOMPOSITION LEVEL FOR UP-SAMPLERS PROPOSED ALGORITHM AND NUMBER OF UP-SAMPLERS ARE ALL SET AS 1

Fusion algorithms	<i>SD</i>	<i>NFMI</i>	<i>Qabf</i>
DWT	50.5549	0.8623	0.4489
CVT	49.7091	0.8614	0.4159
Proposed	<b>68.3933</b>	<b>0.8736</b>	<b>0.6129</b>

TABLE II. PERFORMANCE COMPARISON FOR MEDICAL IMAGES WITH DECOMPOSITION LEVEL / NUMBER OF SCALES = 4 FOR DWT/CVT, AND DECOMPOSITION LEVEL = 1 FOR THE PROPOSED ALGORITHM

Fusion algorithms	<i>SD</i>	<i>NFMI</i>	<i>Qabf</i>
DWT	60.4533	0.8635	0.5354
CVT	57.4019	0.8712	0.5206
Proposed	<b>68.3933</b>	<b>0.8736</b>	<b>0.6129</b>

In order to quantify the fusion performance, popular three metrics, Standard Deviation (*SD*), normalized feature mutual information (*NFMI*) in [17], *Qabf* in [18], are calculated. The three fusion metrics – *SD*, *NFMI*, and *Qabf* – are respectively to measure overall contrast, amount of information obtained from two input images, and overall edge information transferred to the fused image. Results of the three fusion metrics are shown in Table I and Table II. Notice that Table I is the result with decomposition level of 1 for DWT and the proposed algorithm. Similarly, the number of scales for CVT is also set as 1 (i.e., 2 including the coarsest scale) to obtain

Table I. Additionally, since DWT and CVT need to be considered in the same number of subbands in frequency domain, DWT is set with decomposition level of 4, and CVT is also set with 4 for the number of scales, while keeping the proposed algorithm with decomposition level of 1. Those results are in Table II. As shown in Table I and Table II, the proposed algorithm outperforms DWT and CVT. Significant performance improvements are noticed in the proposed algorithm visually as shown in Fig. 4 and numerically as shown in Table I/Table II. Particularly, the proposed algorithm significantly improves transferred edge information and contrast respectively measured by *Qabf* and *SD*.

The proposed algorithm is tested further for other images such as infrared and multifocus images. For visual comparison, some sample results of infrared and multifocus images are included in Fig. 5.

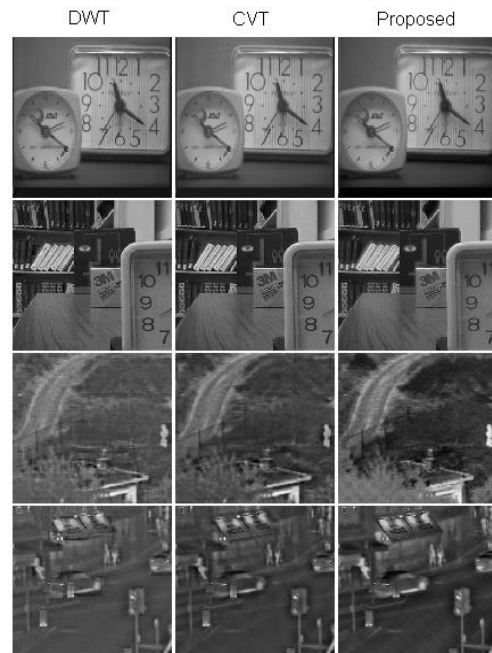


Figure 5. Fusion results for multifocus (1<sup>st</sup> and 2<sup>nd</sup> rows) and infrared (3<sup>rd</sup> and 4<sup>th</sup> rows) images.

Numerical performance measures for infrared and multifocus images are in Table III and Table IV, where total 20 images are tested (i.e., 5 pairs for infrared and multifocus images). Visual results in Fig. 5 and numeral results in Table III/Table IV show that the proposed algorithm is also comparable with DWT and CVT fusion algorithms for infrared and multifocus images as well, even with the simple fusion rule at decomposition level of 1.

TABLE III. PERFORMANCE COMPARISON FOR INFRARED IMAGES WITH DECOMPOSITION LEVEL /NUMBER OF SCALES = 4 FOR DWT/CVT, AND DECOMPOSITION LEVEL = 1 FOR THE PROPOSED ALGORITHM

Fusion algorithms	<i>SD</i>	<i>NFMI</i>	<i>Qabf</i>
DWT	38.6844	0.8821	<b>0.5949</b>
CVT	37.2353	<b>0.8903</b>	0.5774
Proposed	<b>39.2101</b>	0.8798	0.5923

TABLE IV. PERFORMANCE COMPARISON FOR MULTIFOCUS IMAGES WITH DECOMPOSITION LEVEL / NUMBER OF SCALES = 4 FOR DWT/CVT, AND DECOMPOSITION LEVEL = 1 FOR THE PROPOSED ALGORITHM

Fusion algorithms	<i>SD</i>	<i>NFMI</i>	<i>Qabf</i>
DWT	<b>54.4329</b>	0.8761	0.7014
CVT	54.1933	<b>0.8792</b>	<b>0.7155</b>
Proposed	52.9928	0.8677	0.7006

## V. CONCLUSIONS

In this paper, a new image fusion algorithm for medical images is proposed by applying the SGWT in OSGFBs with a simple fusion rule. The proposed algorithm utilizes finer spectral decomposition capability attained from OSGFBs, which are designed through graph signal processing. Significant performance improvement for medical images is observed by the proposed algorithm. Furthermore, comparable performance results with other fusion algorithms such as DWT and CVT are also observed by the proposed algorithm for infrared and multifocus images.

## ACKNOWLEDGMENT

This work was supported in part by an internal grant of Eastern Washington University.

## REFERENCES

- [1] S. K. Narang and A. Ortega, "Perfect reconstruction two-channel wavelet filter banks for graph structured data," *IEEE Trans. on Sig. Process.*, vol. 60, no. 6, pp. 2786-2799, Jun. 2012.
- [2] A. Sandryhaila and J. M. F. Moura, "Discrete signal processing on graphs," *IEEE Trans. on Sig. Process.*, vol. 61, no. 7, pp. 1644-1656, Apr. 2013.
- [3] D. Shuman, S. K. Narang, P. Frossard, A. Ortega, and P. Vandergheynst, "The emerging field of signal processing on graphs," *IEEE Sig. Process. Magazine*, pp. 83-98, May 2013.
- [4] S. K. Narang and A. Ortega, "Compact support biorthogonal wavelet filterbanks for arbitrary undirected graphs," *IEEE Trans. on Sig. Process.*, vol. 61, no. 19, pp. 4673-4685, Oct. 2013.
- [5] A. Sandryhaila and J. M. F. Moura, "Discrete signal processing on graphs: Frequency analysis," *IEEE Trans. on Sig. Proc.*, vol. 62, no. 12, pp. 3042-3054, Jun. 2014.
- [6] Y. Tanaka and A. Sakiyama, "M-Channel oversampled graph filter banks," *IEEE Trans. on Sig. Process.*, vol. 62, no. 14, pp. 3578-3590, Jul. 2014.
- [7] A. Sakiyama and Y. Tanaka, "Oversampled graph Laplacian matrix for graph filter banks," *IEEE Trans. on Sig. Proc.*, vol. 62, no. 24, pp. 6425-6437, Dec. 2014.
- [8] Y. Liu, S. Liu, and Z. Wang, "A general framework for image fusion based on mult-scale transform and sparse representation," *Information Fusion*, vol. 24, pp. 147-164, Jul. 2015.
- [9] H. Li, B. S. Manjunath, and S. K. Mitra, "Multisensor image fusion using the wavelet transform," *Graphical Models and Image Processing*, vol. 57, no. 3, pp. 235-245, May 1995.
- [10] B. Yang, S. Li, and F. Sun, "Image fusion using nonsubsampling contourlet transform," in *Proc. 4th Int. Conf. on Image and Graphics*, 2007, pp. 719-724.
- [11] Q. Zhang and B. Guo, "Multifocus image fusion using the nonsubsampling contourlet transform," *Signal Processing*, vol. 89, no. 7, pp. 1334-1346, 2009.
- [12] M. Choi, R. Y. Kim, M. R. Nam, and H. O. Kim, "Fusion of multispectral and panchromatic satellite images using the curvelet transform," *IEEE Geoscience and Remote Sensing Lett.*, vol. 2, no. 2, pp. 136-140, Apr. 2005.
- [13] F. Nencini, A. Garzelli, S. Baronti, and L. Alparone, "Remote sensing image fusion using the curvelet transform," *Information Fusion*, vol. 8, no. 2, pp. 143-156, Apr. 2007.
- [14] L. Tessens, A. Ledda, A. Pizurica, and W. Philips, "Extending the depth of field in microscopy through curvelet-based frequency-adaptive image fusion," in *Proc. IEEE International Conf. on Acoustics, Speech and Sig. Process.*, Hawaii, USA, 2007, pp. 1861-1864.
- [15] D. K. Hammond, P. Vandergheynst, and R. Gribonval, "Wavelets on graph via spectral graph theory," *Applied and Computational Harmonic Analysis*, vol. 30, no. 2, pp. 129-150, Mar. 2011.
- [16] A. Sakiyama and Y. Tanaka, "Edge-Aware image graph expansion methods for oversampled graph Laplacian matrix," in *Proc. IEEE Int. Conf. on Image Process.*, Paris, France, Oct. 2014.
- [17] M. B. A. Haghighat, A. Aghagolzadeh, and H. Seyedarabi, "A non-reference image fusion metric based on mutual information of image features," *Computers and Electrical Engineering*, vol. 37, no. 5, pp. 744-756, Sept. 2011.
- [18] C. S. Xydeas and V. Petrovic, "Objective image fusion performance measure," *Electronics Letters*, vol. 36, no. 4, pp. 308-309, Feb. 2000.



**Min-Sung Koh** obtained his Ph.D. in Electrical Engineering at Washington State University in Pullman, WA, USA. He was with KEPCO (Korea Electric Power Co.) for 9 years before enrolling in the Ph.D. program at Washington State University. In 2002, he joined the Department of Engineering and Design at Eastern Washington University in Cheney, WA, USA. He is now a full professor of Electrical Engineering at Eastern Washington University.

His research interests include speech/image signal processing, adaptive signal processing, matrix theories, multivariate statistical analysis, signal processing on graphs, brain computer interface, hardware implementation of signal processing algorithms, and signal processing in communication systems.